EXPERIMENTAL INVESTIGATIONS OF LATERAL FORCES INDUCED BY FLOW THROUGH MODEL LABYRINTH GLANDS

Y. M. M. Salman Leong
Universiti Teknologi Malaysia
Jalan Gurney, Kuala Lumpur
Malaysia

R. David Brown
Heriot-Watt University
Riccarton, Edinburgh EH14 4AS
Scotland

A research programme has been undertaken to investigate the lateral forces induced by flow through model labyrinth glands. Circumferential pressure distributions, lateral forces and stiffness coefficients data obtained experimentally are presented and discussed. The force system can be represented as a negative spring and a tagential force orthogonal to eccentricity. The magnitude of these forces were dependent on eccentricity, entry swirl, rotor peripheral velocity and seal size. Tests with a pressure equalisation chamber at mid-gland resulted in significantly reduced forces and stiffness coefficients.

INTRODUCTION

The increase in power density of turbomachinery has highlighted the need to consider more carefully the various excitation mechanisms that may result in high level subsynchronous vibrations. Labyrinth seals are a possible cause of self-excited vibration. The reduction of leakage in turbomachinery has often been sought after for efficiency improvements. Seal clearances and its overall dimensions have been made smaller to achieve this improvement. However undue attention to low leakage may result in unacceptably high forces acting on the rotor. Rotors on the other hand have become relatively more flexible and consequently more susceptible to excitations. Thus a potentially highly efficient machine may prove unreliable in service.

Examples of instabilities thought to be caused by labyrinth seals have been reported in the literature (ref. 1,2). The subsynchronous vibrations observed on operational machines were highly load dependent and the instability frequency greater than half speed. Evidently the destabilising force re-excites the lower criticals.

The possibility of lateral vibrations from labyrinth seal leakage flow dates back to the pioneering work of ALFORD (ref. 3). Efforts had been made to quantify the instability in the literature (ref. 4,5,6,7). However most of this work lacks experimental verification. There is a definite need for more experimental data to assess the nature and significance of these labyrinth leakage flow induced instabilities. Experimental tests on single stage labyrinth gland have been reported by WRIGHT (ref. 8). However extrapolation of single stage labyrinth results to the more practical multistage labyrinths would not be conclusive due to

V_s m/s	Big seals (Set A)				Small seals (Set C & D)			
	U = 0		U = 94 m/s		U = 0		U = 94 m/s	
	K_{xx}^*	K_{xy}^*	K_{xx}^*	K_{xy}^*	K_{xx}^*	K_{xy}^*	K_{xx}^*	K_{xy}^*
0	-0.188	0.000	-0.188	-0.017	-0.081	-0.038	-0.113	-0.109
6	-0.225	0.023	-0.233	0.000	-0.105	0.013	-0.135	-0.113
23	-	-	-	-	-0.075	0.041	-0.124	-0.105

Table 1. Typical dimensionless stiffness coefficients

	BENCKERT et al			GREATHEAD et al		CURRENT WORK	
Labyrinths & Number of Stages	Stepped m = 11	Stepped m = 11	Plain m = 18	Combination m = 24	Combination m = 12	Plain m = 12	Set D
U at which K^* evaluated	0	0	0	N/A	N/A	0	94.3 m/s
$\tilde{E}_{swirl}^*$	0.011	0.072	0.004 ~0.100	N/A	N/A	0.005	0.005
K_{xx}^*	-0.100	-0.067	N/A	-0.010	-0.009	-0.075	-0.124
K_{xy}^*	0.067	0.133	0.090 ~0.720	0.040	0.012	0.041	-0.105

N/A : *Details not available from the text*

Table 2. Comparison of dimensionless stiffness coefficients with other works (ref. 10 and 12)

the interaction in behaviour of the various chambers within in the gland. As this current work and work elsewhere (ref. 9) has shown, the first chamber in a multi-stage gland has a unique behaviour. The work of BENCKERT et al (ref. 9,10) represents the first comprehensive work on multistage labyrinths. The tests and results reported here complement the work of Benckert et al.

NOTATION

e	eccentricity	r	rotor radius
Ecc, ε	eccentricity ratio (e/δ)	U	rotor peripheral velocity
E_{swirl}	swirl energy index	V_s	entry swirl velocity
F	force	θ	peripheral angle, measured from maximum gap
K	stiffness coefficient	ρ	density
L	pitch of labyrinth fins	δ	radial clearance
m	number of stages	Δ	difference
p	absolute pressure	ω	angular velocity
p_o	absolute pressure at inlet		
p_m	absolute pressure at exit		

Subscripts		Superscripts	
i	counter	*	dimensionless
max	maximum	-	mean
r	radial		
t	transverse		
x,y	cartesian coordinates		

EXPERIMENTAL PROGRAMME

An experimental programme to investigate lateral forces resulting from flow through model labyrinth glands has been undertaken. The objectives and philosophy of the programme had been discussed in the previous workshop, NASA CP 2250 (ref. 11). A test rig was designed and manufactured for these investigations. A rigid rotor with rigid bearings was used: this eliminated shaft flexibility and hydodynamic effects. The fundamental mode of measurement was pressure rather than force as it is the unequal pressure field that is responsible for the instability. Static circumferential pressures were measured at 30° intervals at every sealing stage; these measurements were taken off the stator. Figure 1 gives the schematic diagram

of the test bed, and figure 2 the assembly drawing of the test rig. For scaling and cross comparison of various seal geometry, experimental and operational, a seal length parameter was used; defined as

$$\text{seal length parameter} = \frac{\text{cross sectional area of labyrinth chamber}}{\text{rotor radius}}$$

The geometry used was verified to have a length parameter value within those found in operational steam turbines, with the exception of a particular geometry that was made larger to determine the effect of size variation. The various geometry and sealing arrangement used is given in figure 3. Set A and B are those with a big seal dimension. Although the number of stages used could be varied to any combination sealing stages of 12 and 6 were used for the tests. The small seals, set C and D, are as shown; set D being the same as C except with a much higher entry swirl velocity. A series of tests were done with a pressure equalisation chamber in the form of a mid-gland plenum to investigate the effect of such an arrangement. The previous seal set was used and the mid-gland plenum as shown, set E. A short gland arrangement was also used for the smaller seals, set F; and finally a combination seal arrangement, set G. Tests were done with low and moderate entry swirl ($V_s < U_{max}/3$). To obtain a swirl greater than this would necessitate the use of nozzles; this was not used as to avoid a possible pressure bias at entry to the gland.

The experimental parameters were hence

(i) seal geometry

(ii) number of stages

(iii) inlet flow conditions (swirl)

(iv) eccentricity

(v) rotor peripheral velocity.

Figure 4 gives the sign convention adopted for peripheral angle, eccentricity and forces. The circumferential pressure distributions were numerically integrated to obtain forces. A dimensionless force was defined, where

$$F_{r_i}^* = \int_0^{2\pi} \frac{(p \cos\theta \, d\theta)_i}{(p_o - p_m)} \qquad (1.a)$$

$$F_{t_i}^* = \int_0^{2\pi} \frac{(p \sin\theta \, d\theta)_i}{(p_o - p_m)} \qquad (1.b)$$

$$\text{Hence } F_{r,t_i} = F_{r,t_i}^* \times r_i L (p_o - p_m) \qquad (2)$$

and

$$\text{Resultant force } F = \sum_{i=0}^{m} F_i \qquad (3)$$

Note that no extraneous sign was introduced in the relations. A positive radial force is a decentreing force (negative spring force) and a negative radial force a restoring force. A positive transverse force is a forward whirl force.

The stiffness coefficients are as conventionally defined;

$$\text{Direct stiffness coefficient i.e. restoring force coefficient} \quad K_{xx}^* = \frac{-\Delta F_r^*}{\Delta \varepsilon} \qquad (4.a)$$

and Cross-coupled stiffness coefficient $K_{xy}^* = \dfrac{F_t^*}{\Delta \varepsilon}$ (4.b)

Assuming linearity,

$$| K_{yy}^* | = | K_{xx}^* |$$

$$| K_{yx}^* | = -| K_{xy}^* | \qquad (5)$$

Also $$K = K^* r L (\bar{p}_o - \bar{p}_m) / e \qquad (6)$$

EXPERIMENTAL RESULTS

Circumferential Pressure Distributions

Examples of the circumferential pressure distributions, normalised against the pressure drop across the gland, are given in figures 5 - 8. The pressure distribution for the large seals (set A) is as shown, figure 5. Moderate asymmetric pressure field does exist, with consistently regular semi-symmetric suction pressure in all the chambers beyond the first chamber; the first chamber having a positive pressure field. The smaller seals (set D) had a very much more significant asymmetric pressure field, figure 6. The positive pressure in the first chamber was still observed. Beyond the chambers at the entry end unsymmetric suction pressure fields were obtained, with chambers towards the exit end developing a larger sinusoidal component. The introduction of a plenum chamber in the mid-gland of the same seal set (set E) shows a significant alteration to the pressure field, figure 7. The circumferential pressure variation in the chambers prior to the plenum was reduced. The chamber immediately after the plenum (i.e. chamber number 7) now behaved as a "first chamber" in a normal gland assembly, thereby breaking down the build up of the pressure field in the stages along the gland. In the sealing arrangement with a lesser number of stages, set F, the pressure variation was greater than the long glands, figure 8. This was obvious as the axial pressure drop per stage was larger.

In the larger seal geometry, set A and B, there was no appreciable circumferential pressure variation for zero eccentricity, as should be the case. However in the

smaller seals, significant residual asymmetric field did exist at zero eccentricity. It was not thought to be due to pecularities in the individual seal unit or alignment and concentricity as these were thoroughly checked and verified. These residual pressure fields were thought to be caused by flow dissymmetry resulting from a random build effect and random variations in the actual fin clearances; the chambers were sufficiently small as not to allow pressure equalisation. Such an occurrence had also been noted by Greathead et al on a scaled model rig of an operational machine (ref. 12).

Lateral Force Distributions

The graph of dimensionless force (pressure coefficient) plotted against seal chamber number for the large seals, set A, is given in figure 9. An immediate observation was that variation did exist in the force levels with respect to chambers. The radial force in the first chamber was a restoring force and beyond this chamber decentreing forces existed. The transverse forces were significantly smaller than the radial forces. Variation due to eccentricity is also indicated. The relatively larger pressure variation of the smaller seals not unnaturally gave higher force levels than the large seals, figure 10. Variation in force levels with chamber number was also observed. In contrast with results from the big seals, the transverse forces were now considerably larger in magnitude, having the same order in magnitude as the radial forces. It does suggest that small seals are potentially more destablising than large seals. What was further obvious was the significant force that existed even at zero eccentricity. Significant variation in the force levels was observed as a result of variation in the rotor velocity, figure 11. The resultant decentreing force increased significantly with rotor velocity, and the resultant transverse force from being a forward whirl force at U = 0 changed to a backward whirl force at high rotor velocity ($U > V_s$). Swirl slightly increased the decentreing force as well as the forward transverse force at U = 0, figure 12.

The comparison of forces for the sealing arrangment with and without the plenum chamber, figure 13, strengthens the observation already seen in the circumferential pressure distributions. The radial force level in the chambers were generally very much reduced, and hence the resultant decentreing force more than halved its previous value. The transverse force was similarly reduced.

Stiffness Coefficients

Negative radial stiffness was generally obtained for most of the seal arrangements; with either forward or backward cross-coupled stiffness: this being dependent on several parameters. Table 1 gives a selection of the dimensionless stiffness coefficients obtained from graphs of dimensionless force plotted against eccentricity ratio.

For the big seals, set A, a relatively large negative radial stiffness coefficient was obtained. The cross-coupled stiffness coefficient was significantly smaller, figure 14. This observation was also true for the short gland seals (set B) of the same geometry, figure 15. High rotor velocity tended to give a backward cross-coupled stiffness coefficient; however at U = 0 ($V_s > U$) increasing swirl resulted in increasing forward cross-coupled stiffness coefficient (positive K_{xy}*). The effect of rotor peripheral velocity on the coefficients is even more evident in the small seals (set C and D), where increasing rotor velocity increases the

negative direct stiffness coefficients, as well as greatly altering the characteristics of K_{xy}*. The transverse force from being a positive (forward whirl) force changed to a negative (backward whirl) force, figure 16. At low or no rotor velocity, increasing swirl rate resulted in increasing forward cross-coupled stiffness coefficient, figures 16 and 17.

The introduction of a mid-gland plenum was seen to have a significant moderating effect on the force levels and the stiffness coefficients, figure 18. Force levels and coefficients were greatly reduced. The previous observation of the effect of swirl and rotor velocity was still true although of lesser influence. The short gland small seals (set F) had positive direct stiffness in contrast with the other seals, figure 19. The cross-coupled stiffness behaved in the same manner as previously observed, i.e. effects due to swirl and rotor peripheral velocity on K_{xy}*. The combination seals (set G) due to its design of small and large chambers showed the influence of size variation on the pressure distributions; and the resulting stiffness coefficients reflected this, figure 20. Variation due to rotor velocity and swirl were again consistent in behaviour.

DISCUSSIONS

Lateral forces do exist as a result of flow through labyrinth glands. These forces generally increased with eccentricity. Significant decentreing radial forces were obtained in all the seal configurations, except for the small short gland with restoring forces. The decentreing forces generally increased with seal size. Transverse forces orthogonal to displacement however are of most interest. Both forward and backward transverse forces were obtained; very much dependent on rotor peripheral velocity, swirl and seal size. The experimental observations suggest that small seals are potentially more destablising than big seals; with the smaller seals yielding a larger cross-coupled stiffness coefficient. This would be consistent with an experience of KIRK (ref. 13) where a rotor instability in a compressor was eliminated by replacing the labyringth seals with seals twice the original dimensions.

The experimental results also suggest the important influence of rotor peripheral velocity on the resultant forces. This effect of rotor velocity was more prominent in the small seals. Increasing rotor velocity generally increased the decentreing force in the glands, and thus gave a negative direct stiffness coefficient. All tests further indicated that increasing rotor velocity resulted in negative cross-coupled stiffness coefficient. If a nett positive transverse force F_t* already exists in the gland (by virtue of swirl for example) then rotor velocity reduces this nett force and could give a negative F_t* (backward whirl force). A strong self-excited backward whirl has been reported by WRIGHT (ref. 8) on a whirling rotor model.

The moderate swirl that was obtained on the current rig indicated an increased positive transverse force (forward whirl) with increased swirl, and yielded a forward cross-coupled stiffness coefficient. This observation was prominent in zero or low rotor velocity tests. However as rotor velocity increases the nett backward transverse force resulting from inertia effects was seen to dominate the forward transverse force originating from entry swirl. Figure 21 gives a plot of dimensionless cross-coupled stiffness coefficient against swirl energy for the small seals (sets C and D). A distinct increase in K_{xy}* with entry swirl energy was observed and indicates the strong dependence of K_{xy} on entry swirl. It is reasonable to suppose that if a higher swirl velocity was used higher values of cross-coupled stiffness coefficient would be obtained. This conclusion on the

influence of entry swirl on the cross-coupled stiffness is in agreement with results obtained by BENCKERT et al with high entry swirl energy (ref. 9, 10). The effect of swirl on the direct stiffness coefficient K_{xx} is not as significant. Table 2 gives a comparison of stiffness coefficients with works elsewhere (ref. 9, 10, 12). Results from this work compares well, recognising in particular that the work done by Benckert et al at extremely high entry swirl was not obtained on the current rig.

In order to appreciate the full significance of the dimensionless parameters seen so far, a K* value of 0.050 on a 83 bar pressure drop, rotor radius 254 mm, labyrinth pitch 8 mm and eccentricity 0.50 mm would give a stiffness coefficient of 1.8×10^6 N/m. Hence if the results from Table 2, $K_{xy}^* = 0.04$ and $K_{xx}^* = -0.004$ and $K_{xx}^* = -0.075$, were to be applied to this typical steam turbine, then the respective coefficients are: $K_{xy} = 1.5 \times 10^6$ N/m and $K_{xx} = -2.7 \times 10^6$ N/m. Values of similar order in magnitude for a steam turbine had been quoted by Benckert et al (ref. 10).

The current work further suggests the importance of the relationship between the rotor peripheral velocity U and the swirl velocity V_s. Apparently when $V_s > U$ a forward cross-coupled stiffness coefficient was obtained and when $V_s < U$ a backward cross-coupled stiffness was obtained instead. This draws parallel to the proposals of ROSENBERG et al (ref. 14) and also as noted by GREATHEAD et al (ref. 15), that a positive transverse force would be obtained when the swirl velocity was greater than the rotor precession, and vice versa.

Results and implications from the tests involving a mid-gland plenum were very interesting. The direct stiffness coefficient was a mere 10% to 15% of previous values without the plenum, and the cross-coupled stiffness coefficients 25% to 45%. Inevitably questions would be asked on the penalty of increased leakage flow resulting from the use of this gland with the plenum. Flowrate measurements monitored on this gland arrangement showed no increase in mass flow for the same pressure head. Such a pressure equalisation chamber is also relatively simple to incorporate in existing operational machines. Suggestions had been made by KOSTYUK et al (ref. 16) on a pressure equalisation stability unit at the entry to the gland in an operational machine; reported of improvement to its instability threshold. The results of this work and by Benckert et al also confirm the wisdom in recent attempts to reduce swirl by the use of vortex brakes (ref. 17).

Shortcomings in existing theories particularly those not predicting forces or instability with parallel rotor displacement were certainly highlighted. Tapered seal clearances (either converging or diverging) are not necessarily a prerequisite for instability. New theoretical attempts to formulate labyrinth forces are required and should accommodate the fact that forces do exist for parallel rotor displacements.

CONCLUSIONS

This current work shows that an assymmetric pressure field does exist in all chambers within a gland assembly, even for parallel eccentricity displacements contrary to what is predicted by existing theories. The lateral forces were dependent on eccentricity, swirl, rotor peripheral velocity and seal size. The force system could normally be represented as a negative spring and a tangential force orthogonal to eccentricity. Both forward and backward cross-coupled stiffness coefficients were obtained, the direction being dependent on the ratio between swirl and rotor peripheral velocity. Small seals were also shown to be

potentially more destabilising. The use of a mid-gland plenum chamber showed marked reduction in forces and stiffness coefficients, without any increase in leakage flow.

REFERENCES

1. Greathead, S.H. and Bastow, P.: Investigations into Load Dependent Vibrations of the High Pressure Rotor on Large Turbo-Generators. I.Mech.E. Conference on Vibrations in Rotating Machinery, September 1976, pp. 279-285.

2. Jenny, R.: Labyrinths as a Cause of Self-Excited Rotor Oscillations in Centrifugal Compressors. Sulzer Technical Review 4/1980, pp. 149-156.

3. Alford, J.S.: Protecting Turbomachinery from Self-Excited Rotor Whirl. Trans. ASME, J.Engng. Power, October 1965, pp. 333-344.

4. Spurk, J.H. and Keiper, R.: Self-Excited Vibration in Turbomachines resulting from Flow through Labyrinth Glands. C.E. Trans. 6785. Translated from Ingenieur Archiv. Vol. 43 (1974), pp. 127-135.

5. Kostyuk, A.G.: A Theoretical Analysis of the Aerodynamic Forces in the Labyrinth Glands of Turbomachines. Thermal Engineering Vol. 19 (11) 1972, pp. 39-44. (Teploenergetika 1972. 19 (11), pp. 29-33).

6. Iwatsubo, T.: Evaluation of the Instability Forces of Labyrinth Seals in Turbines or Compressors. Workshop on Rotordynamic Instability Problems in High-Performance Turbomachinery. Texas A & M Univ., May 1980. NASA Conference Publication 2133, pp. 139-167.

7. Kurohashi, M., Inoue, Y., Abe. T. and Fujikawa, T. : Spring and Damping Coefficients of the Labyrinth Seals. I.Mech.E. Conference on Vibrations in Rotating Machinery, September 1980, pp. 215-222.

8. Wright, D.V.: Air Model Tests of Labyrinth Seal Forces on a Whirling Rotor. Trans. ASME, J.Engng. Power, October 1978, pp. 533-543.

9. Benckert, H. and Wachter, J.: Flow Induced Coefficients of Labyrinth Seals for Application in Rotordynamics. Workshop on Rotordynamic Instability Problems in High-Performance Turbomachinery. Texas A & M Univ., May 1980. NASA Conference Publication 2133, pp. 189-212.

10. Benckert, H. and Wachter, J.: Flow Induced Constants of Labyrinth Seals. I.Mech.E. Conference on Vibrations in Rotating Machinery, September 1980, pp. 53-63.

11. Leong, Y.M.M.S. and Brown, R.D.: Circumferential Pressure Distributions in a Model Labyrinth Seal. Workshop on Rotordynamic Instability Problems in High-Performance Turbomachinery, Texas A & M Univ., May 1982, NASA Conference Publication 2250, pp. 223-241.

12. Greathead, S.H. and Slocombe, M.D.: Further Investigations into Load Dependent Low Frequency Vibration of the High Pressure Rotor on Large Turbo-Generators. I.Mech.E. Conference on Vibrations in Rotating Machinery, September 1980, pp. 401-413.

13. Kirk, R.G.: Private communication, Texas A & M Univ., May 1982.

14. Rosenberg, C.S., Orlik, W.G. and Marshenko, U.A.: Investigating Aerodynamic Transverse Forces in Labyrinth Seals in Cases Involving Rotor Eccentricy. C.E. Trans. 7083. Translated from Energomashinostrojenie Vol. 8, 1974, pp. 15-17.

15. Greathead, S.H. and Slocombe, M.D.: Investigations into Output Dependent Rotordynamic Instability of the High Pressure Rotor on a Large Turbogenerator. IFTOMM Conference on Rotorydynamic Problems in Power Plants, Italy, September 1982, pp. 27-35.

16. Kostyuk, A.G., Pis'min, I.N., Serkov, S.A., ,Shoshin, V.G. and Shatin, S.A.: Raising the Threshold Capacity and Efficiency of Turbine Plants when Using Stabilising Units. Thermal Engineering Vol. 28 (5) 1981, pp. 311. (Teploenergetika 1981 28 (5) pp. 50-53).

17. Jenny, R. and Wyssmann, H.: Lateral Vibration Reduction in High Pressure Centrifugal Compressors. Proceedings 9th Turbomachinery Symposium, Houston, December 1980, pp. 45-56.

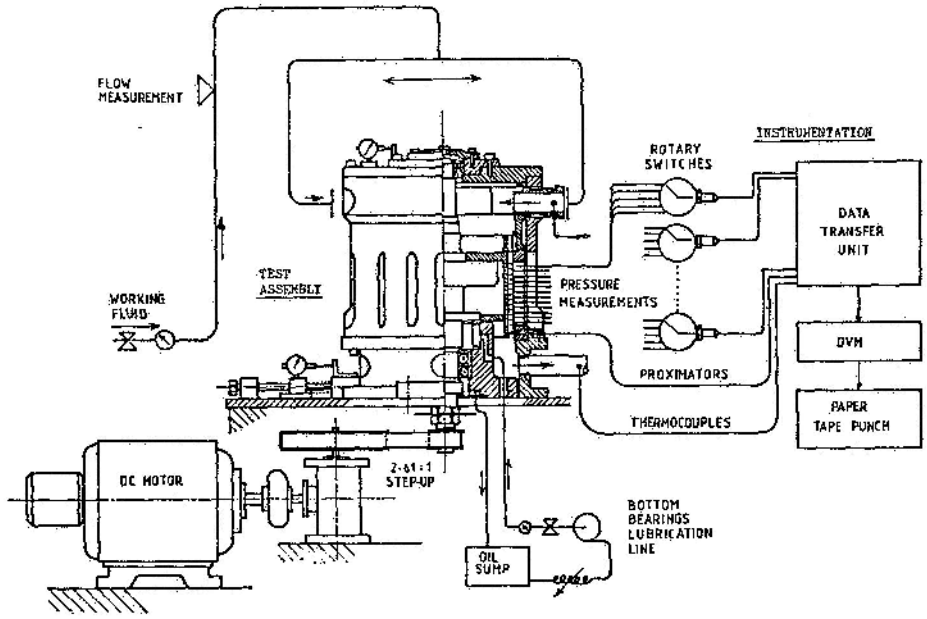

Figure 1. Schematic layout of test bed and instrumentations

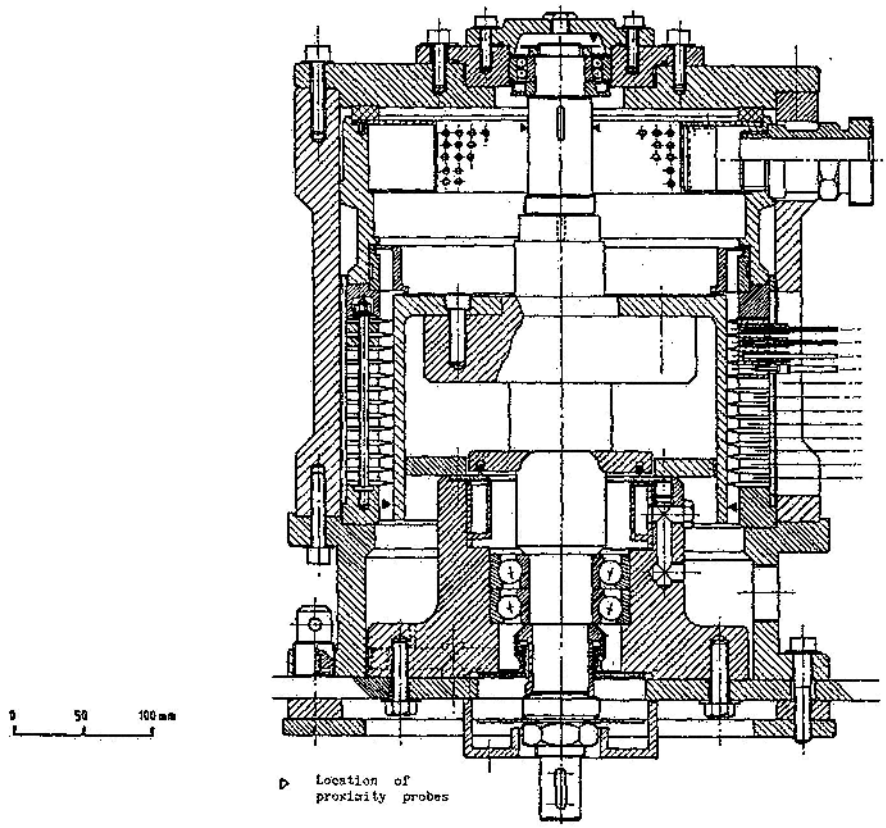

Figure 2. Sectioned assembly drawing of test rig (main assembly)

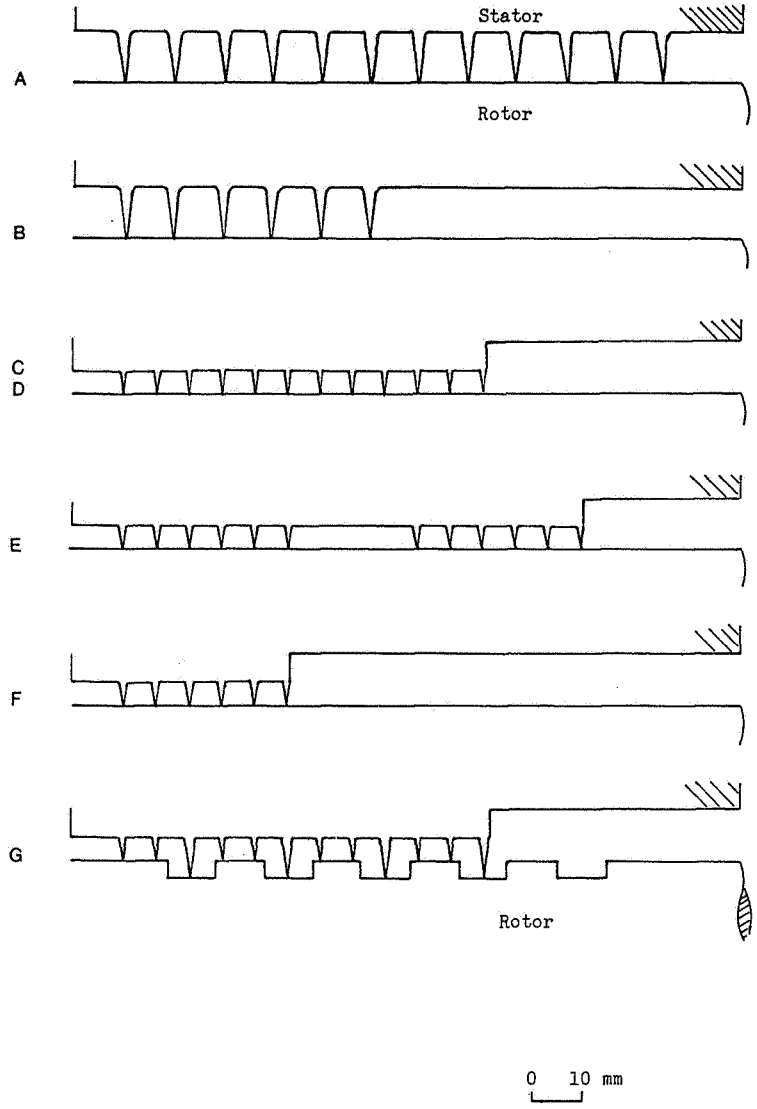

Figure 3. Experimental seal geometry and number of stages of stages combination used

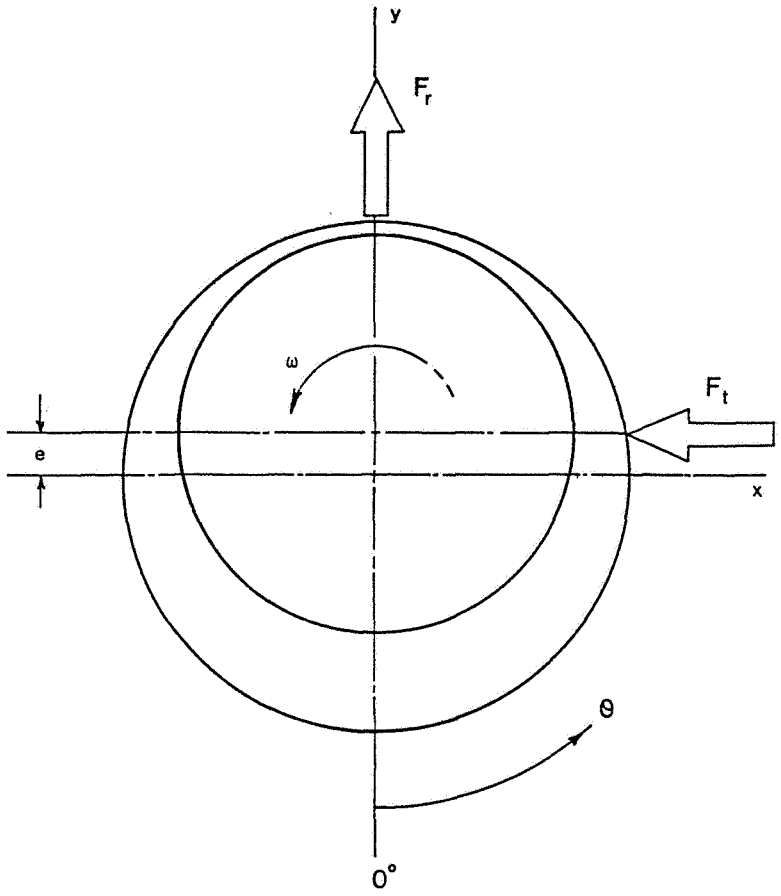

Figure 4. Sign convention of peripheral angle, eccentricity and forces

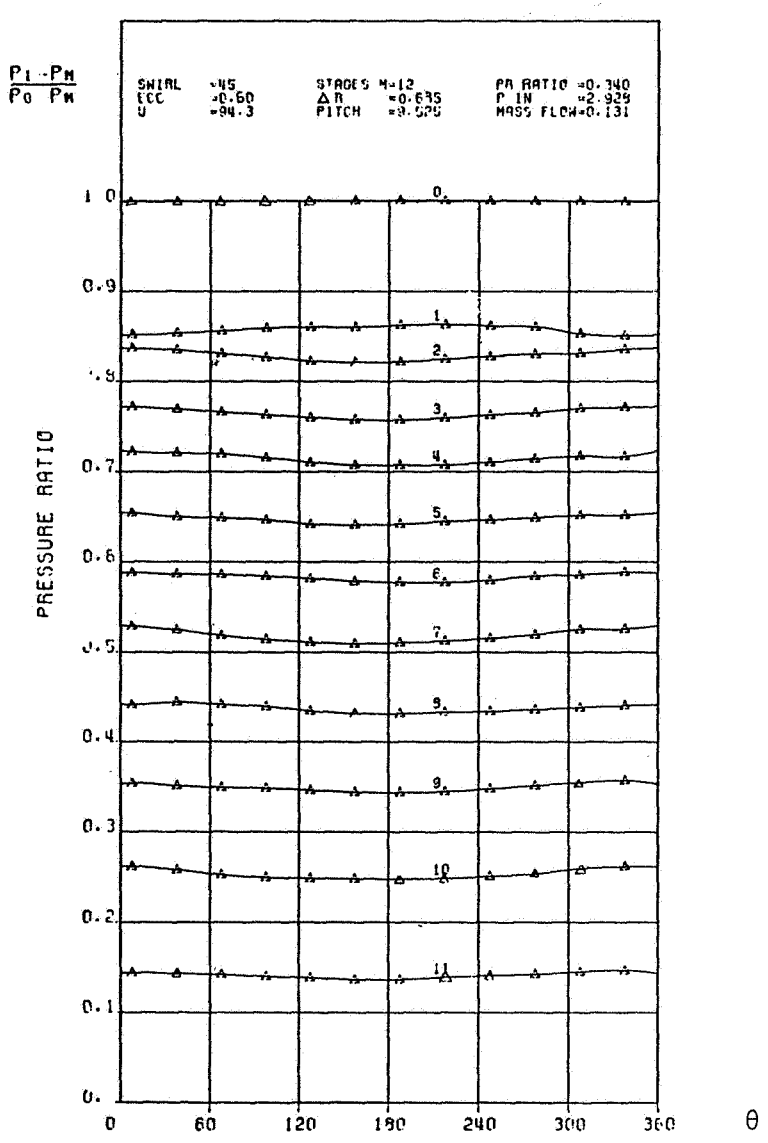

Figure 5. Pressure ratio; set A, $\varepsilon = 0.6$, $U = 94$ m/s, $V_s = 6$ m/s

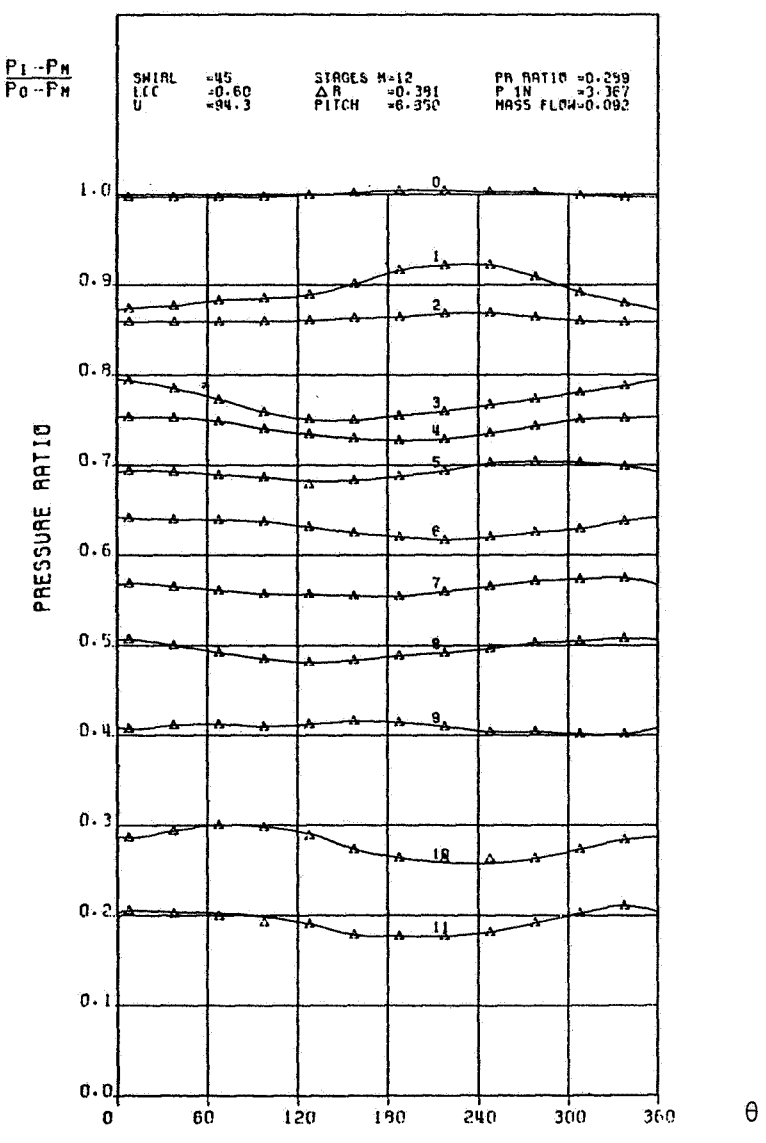

Figure 6. Pressure ratio; set D, $\varepsilon = 0.6$ $U = 94$ m/s, $V_s = 23$ m/s

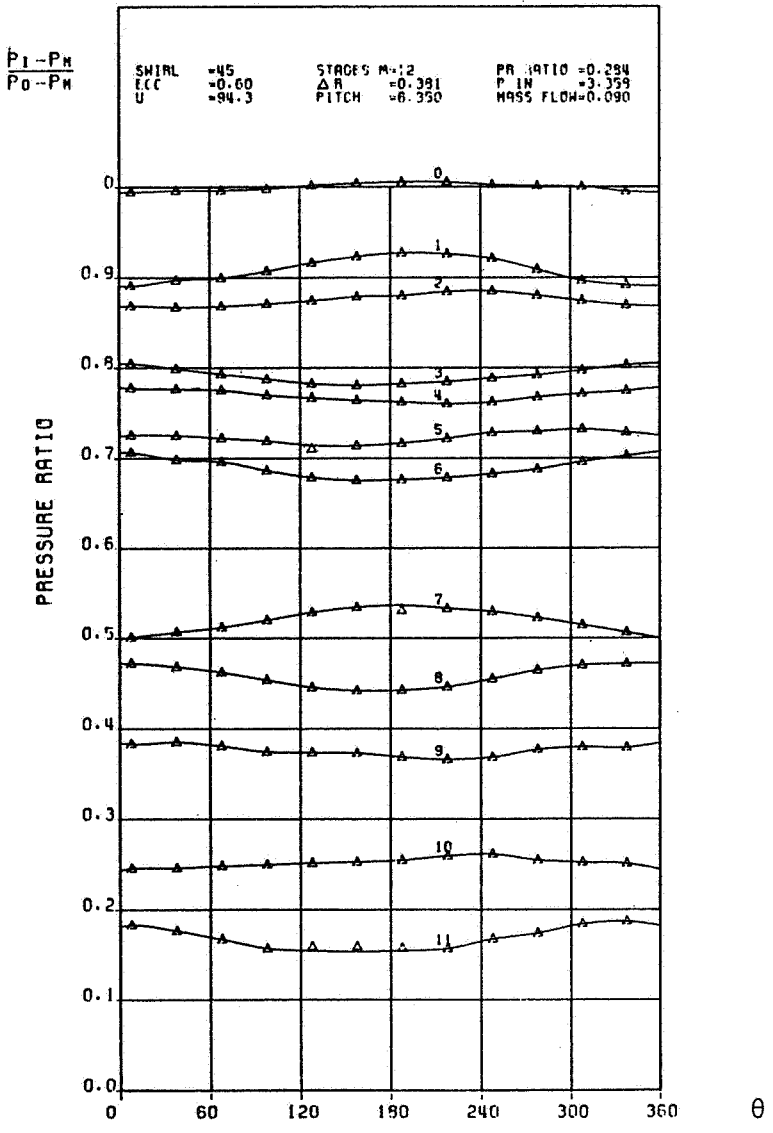

Figure 7. Pressure ratio; set E, $\varepsilon = 0.6$
U = 94 m/s, V_s = 23 m/s

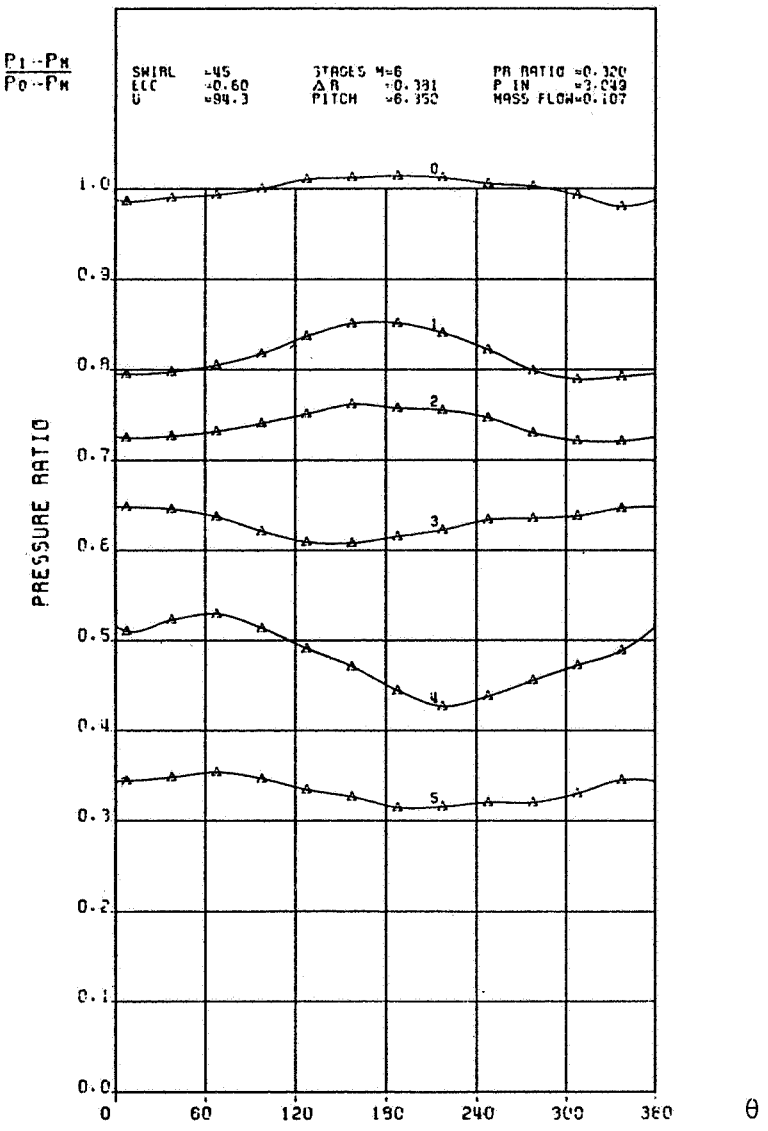

Figure 8. Pressure ratio; set F, $\varepsilon = 0.6$
U = 94 m/s, V_s = 30 m/s

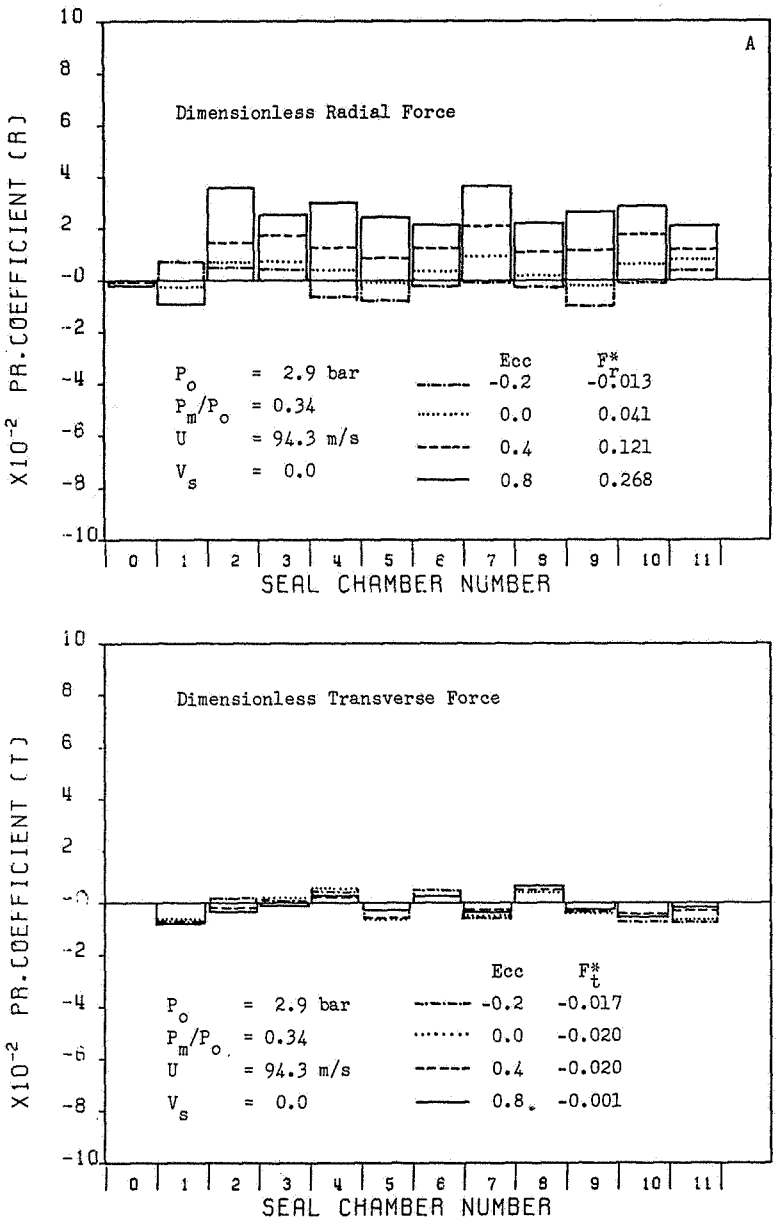

Figure 9. Dimensionless force in individual seal chamber : Effect of eccentricity; set A

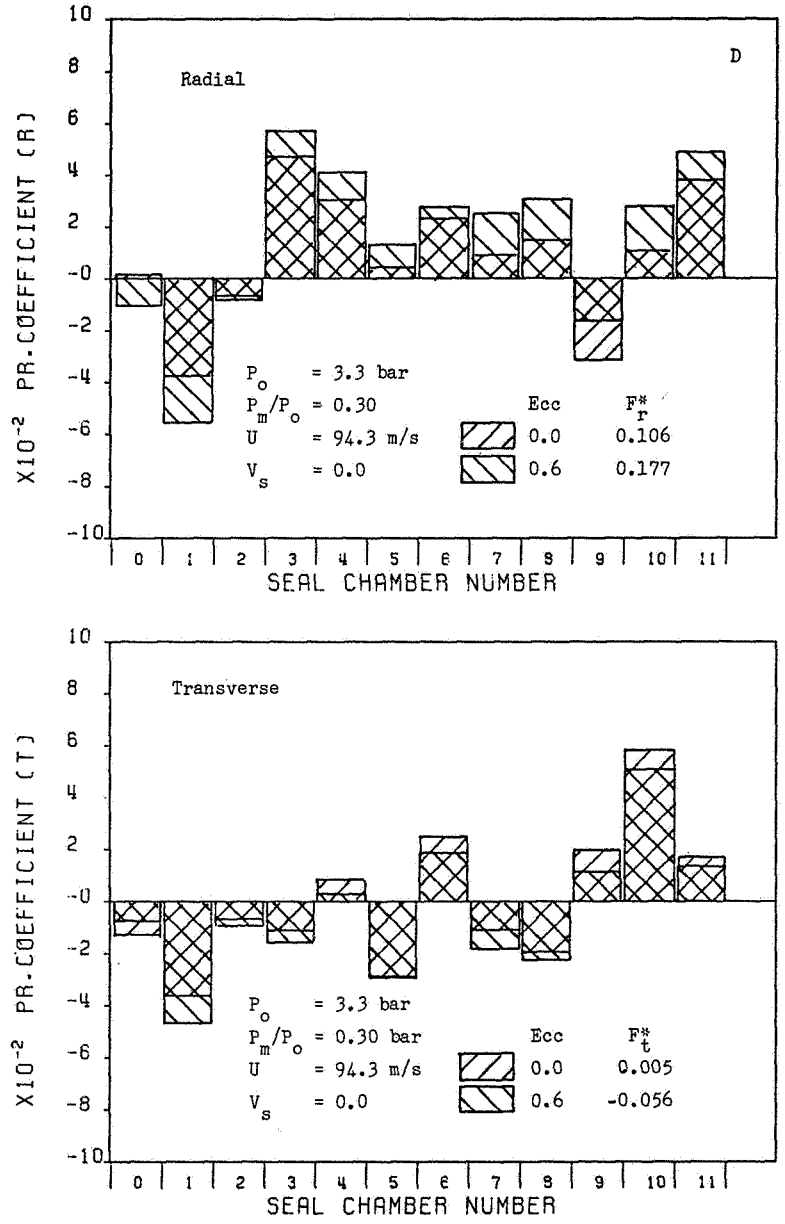

Figure 10. Effect of eccentricity on the dimensionless force; set D

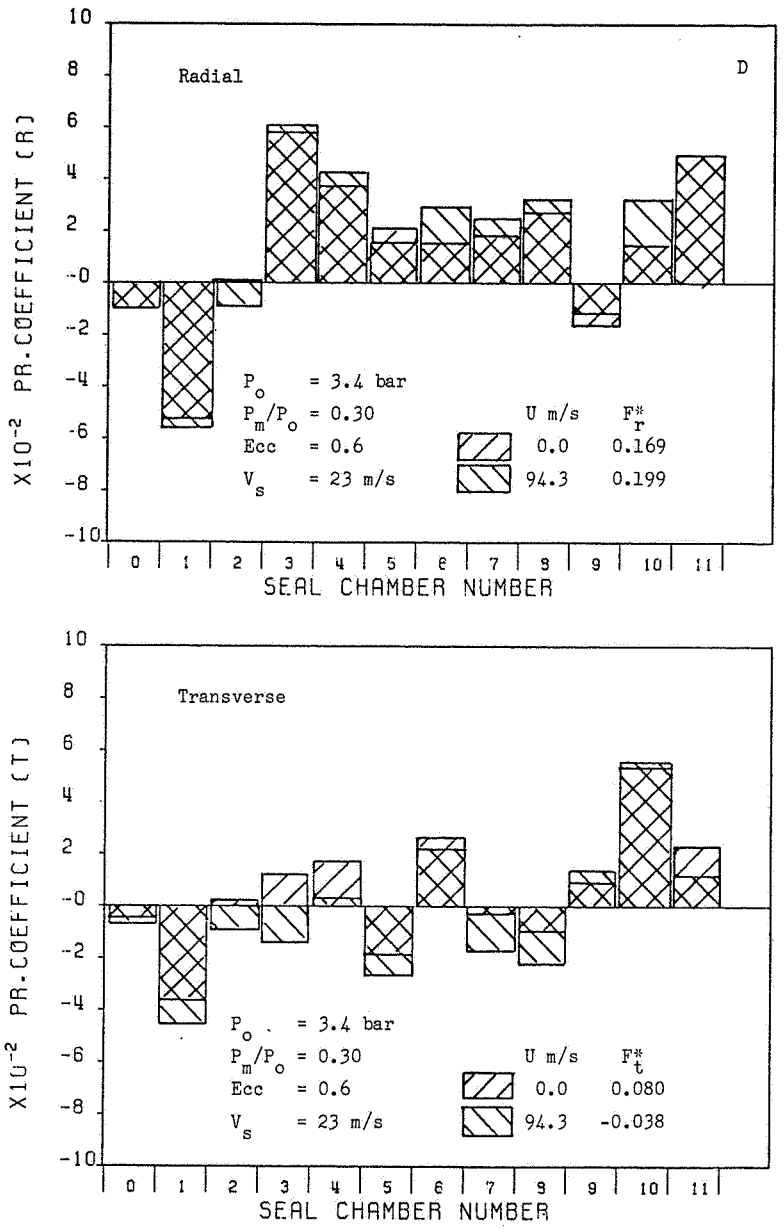

Figure 11. Effect of rotor peripheral velocity on the dimensionless force; set D

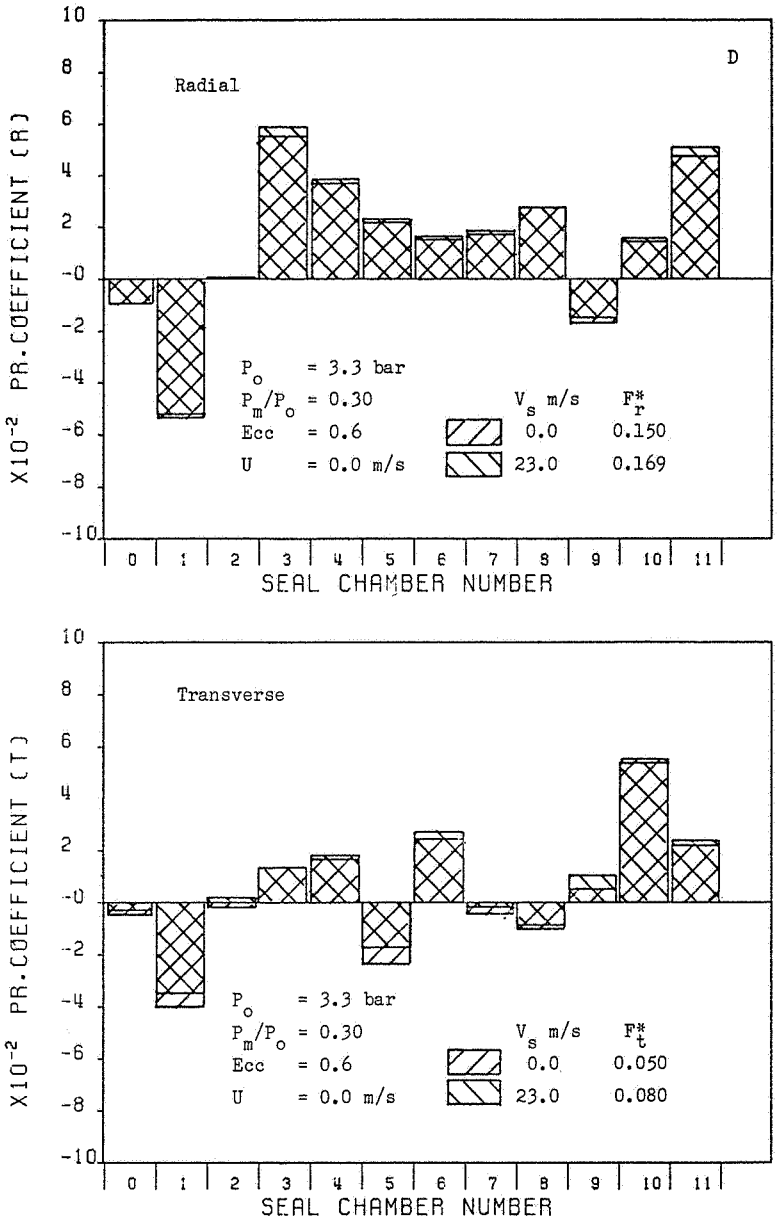

Figure 12. Effect of moderate swirl on the dimensionless force, U = 0; set D

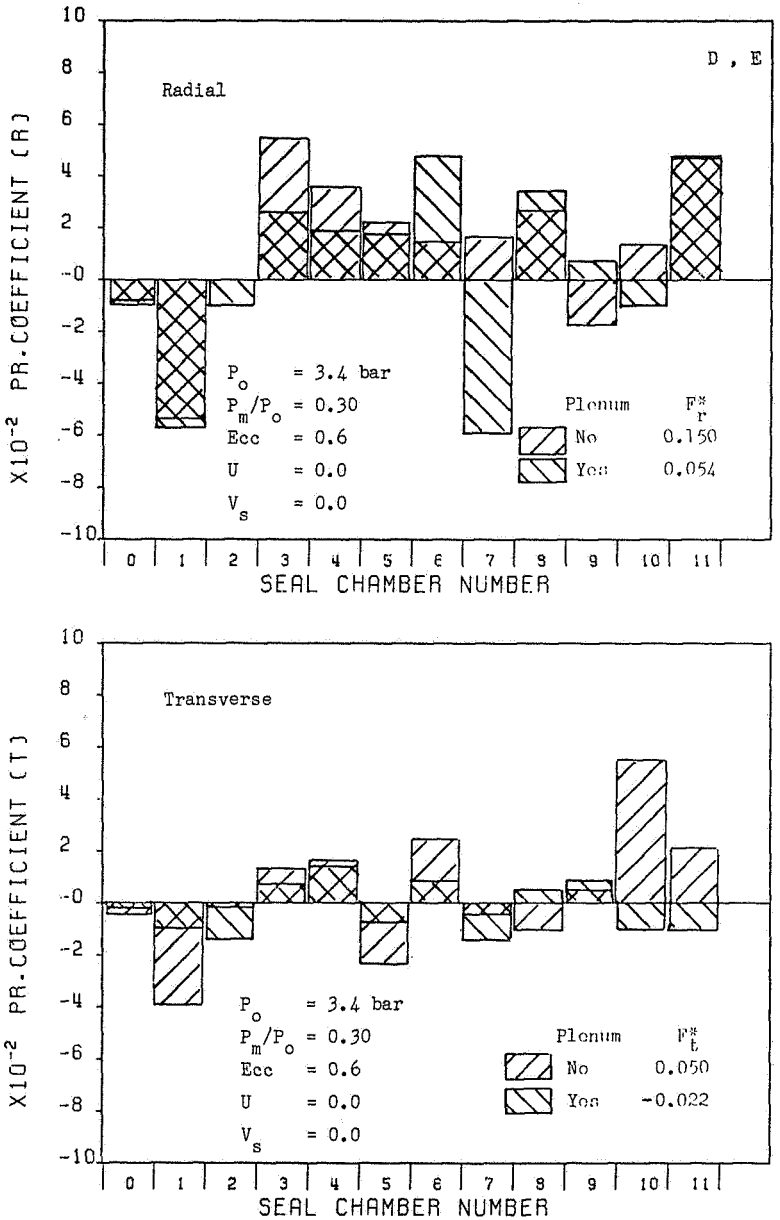

Figure 13. Comparison of dimensionless force with and without mid-gland plenum

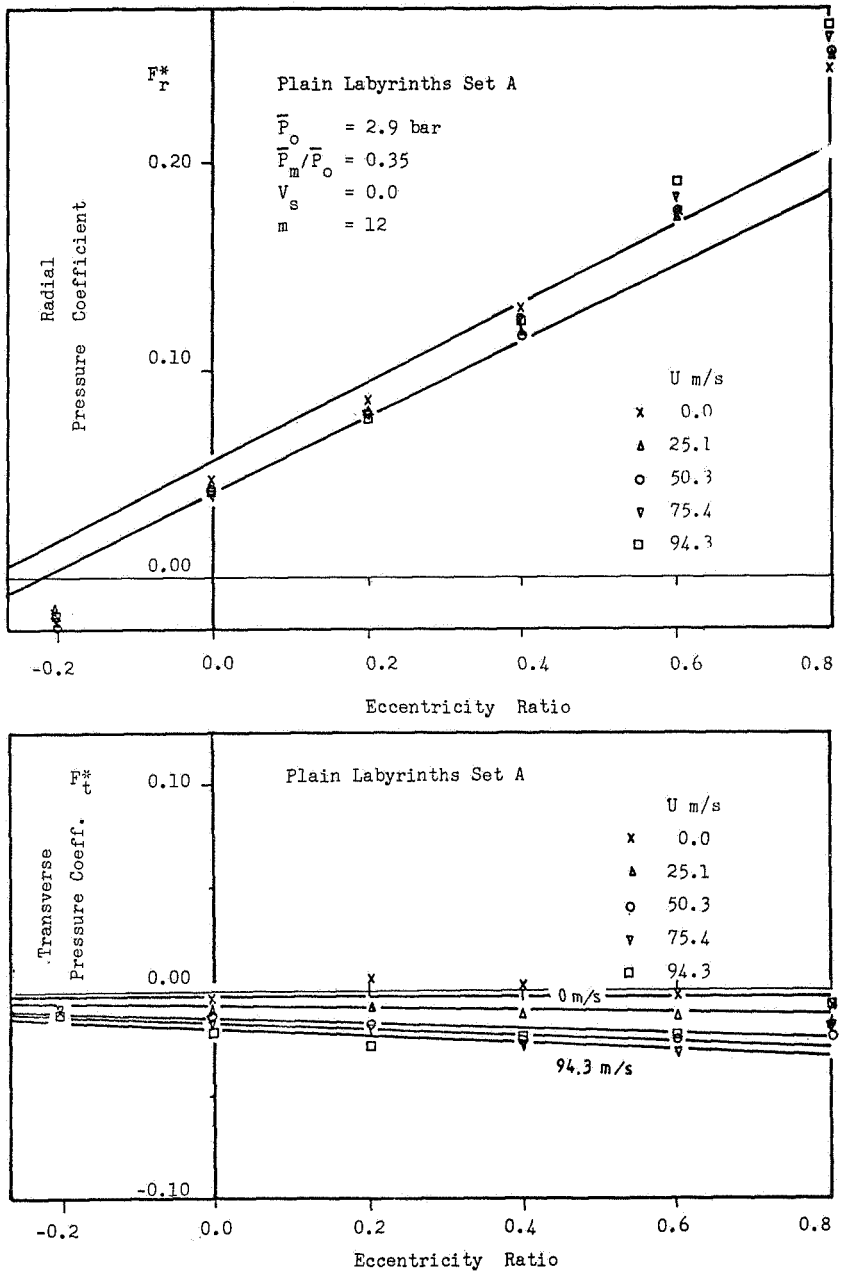

Figure 14. Graphs of dimensionless force against eccentricity ratio; set A, $V_s = 0$

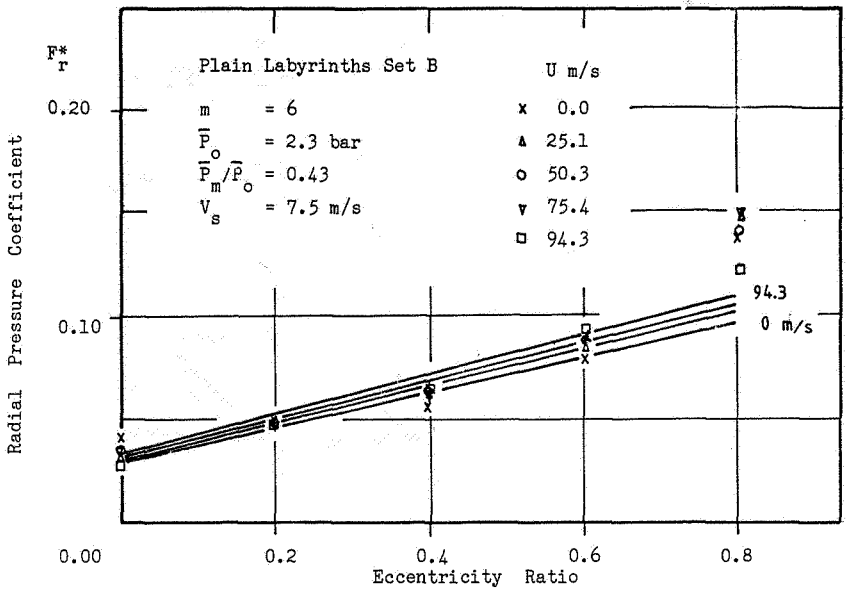

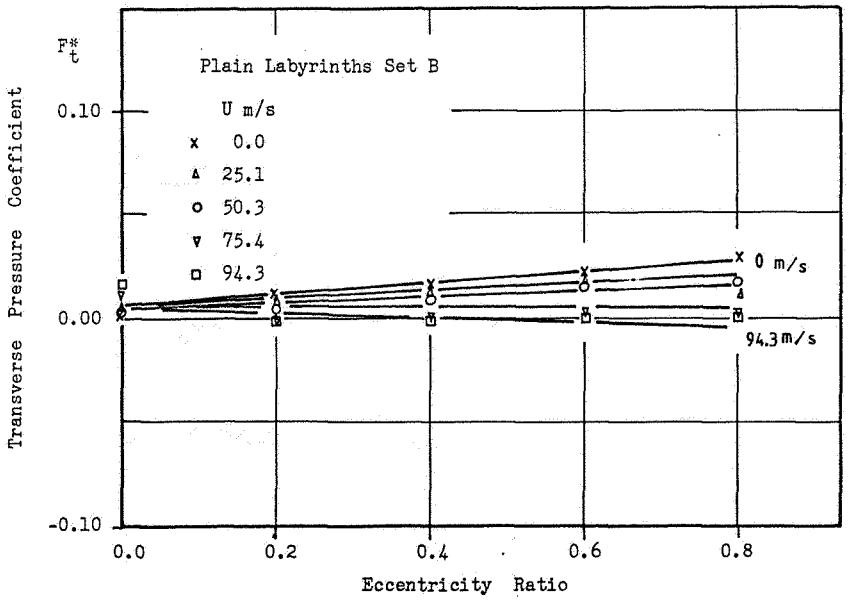

Figure 15. Graphs of dimensionless force against eccentricity ratio; set B, V_s = 7.5 m/s

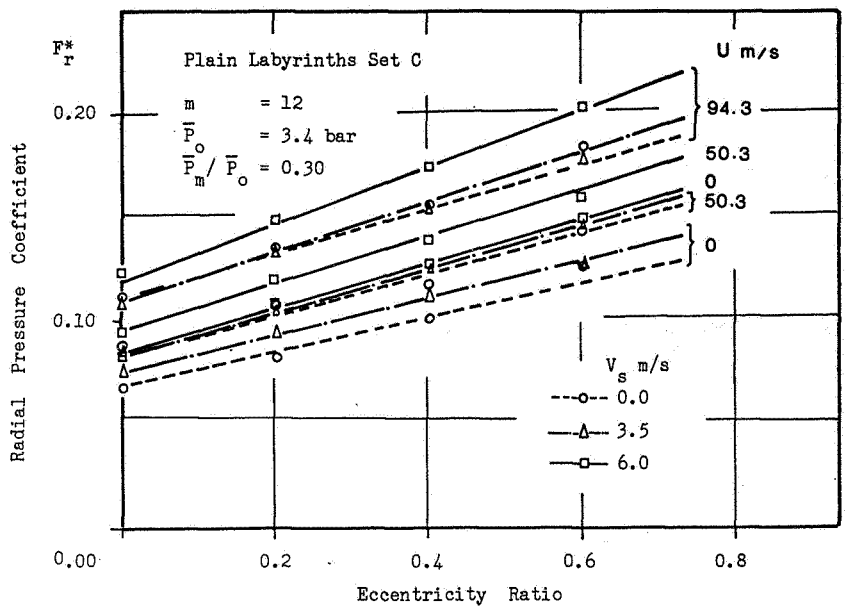

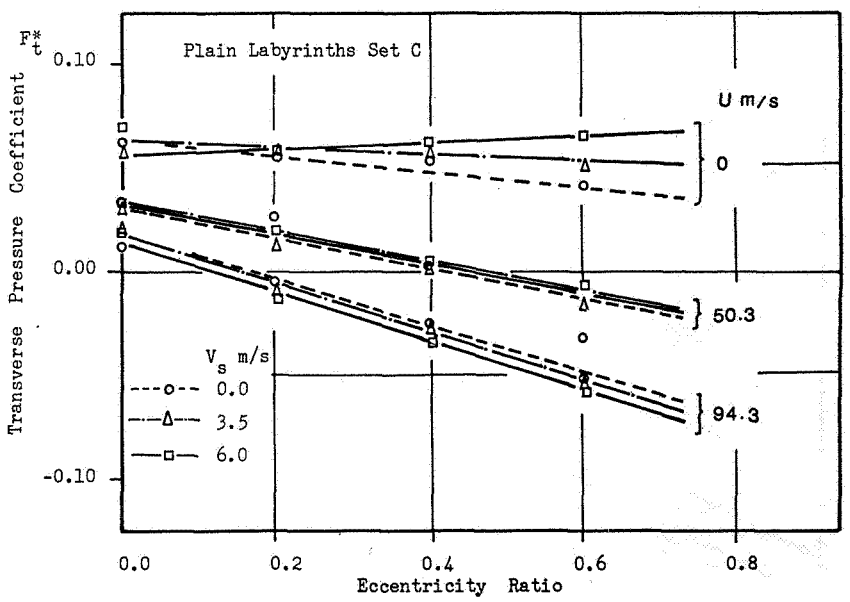

Figure 16. Graphs of dimensionless force against eccentricity ratio; set C

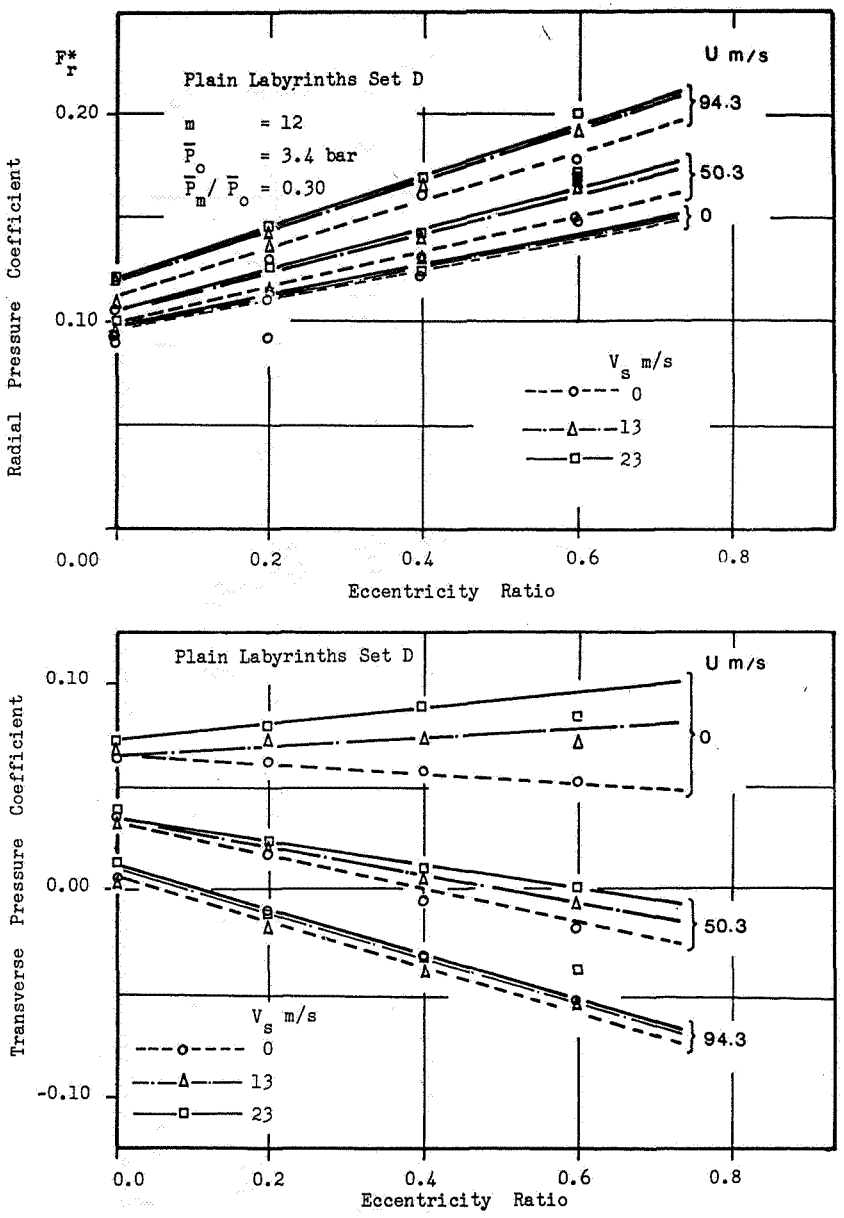

Figure 17. Graphs of dimensionless ratio against eccentricity ratio; set D

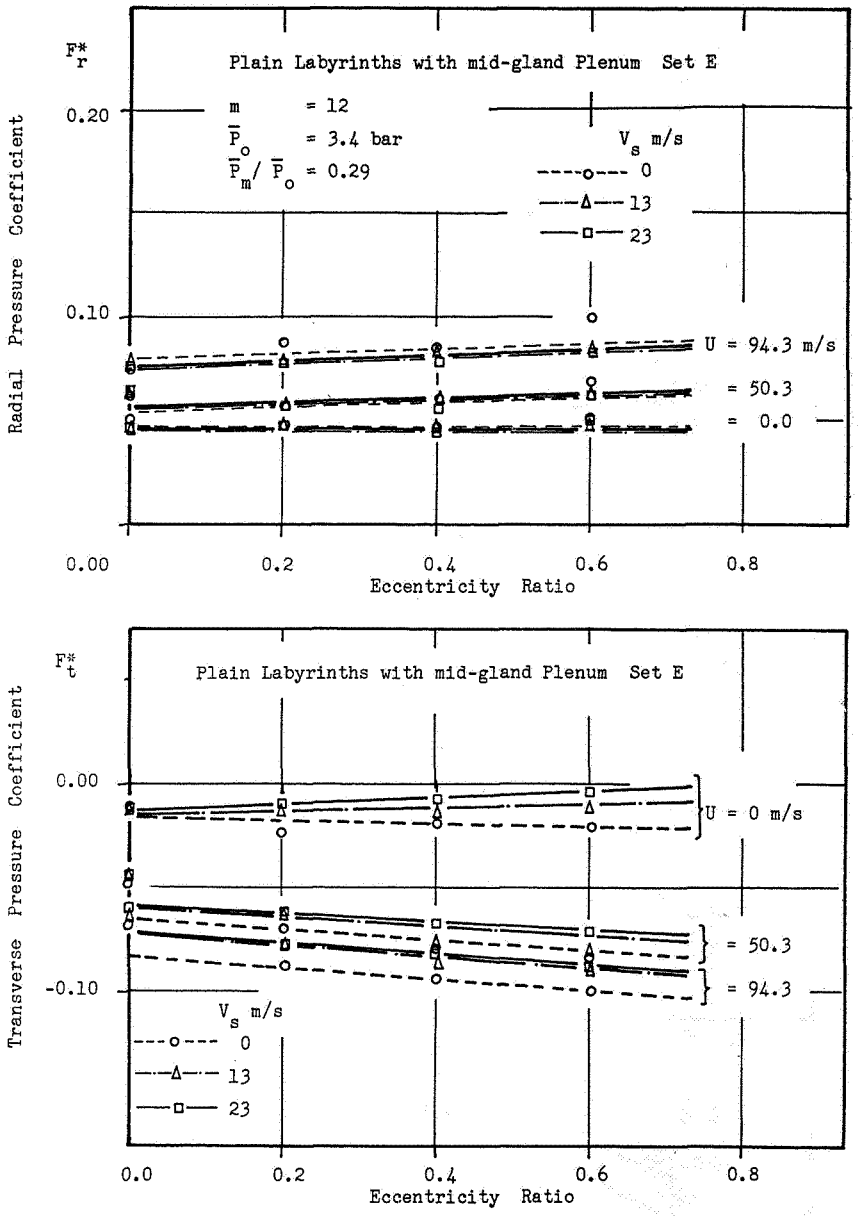

Figure 18. Graphs of dimensionless ratio against eccentricity ratio; set E

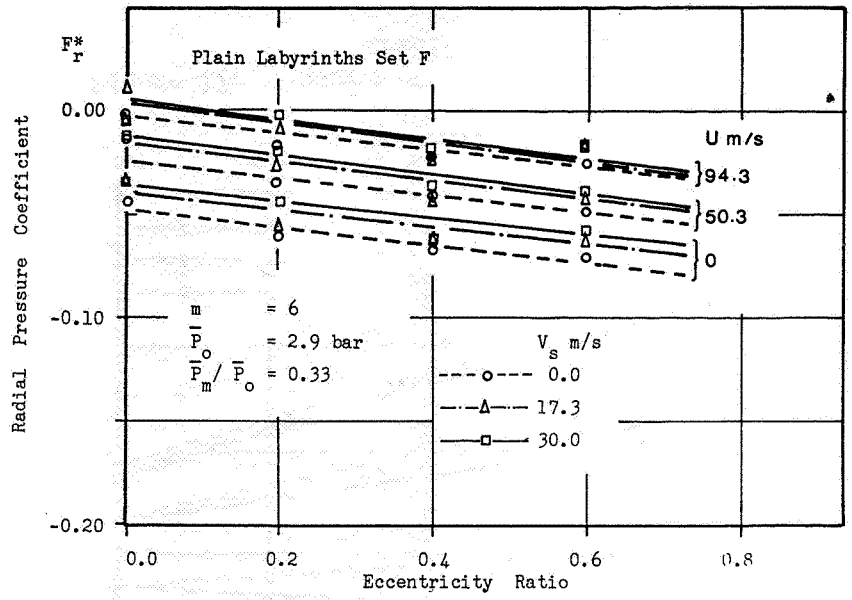

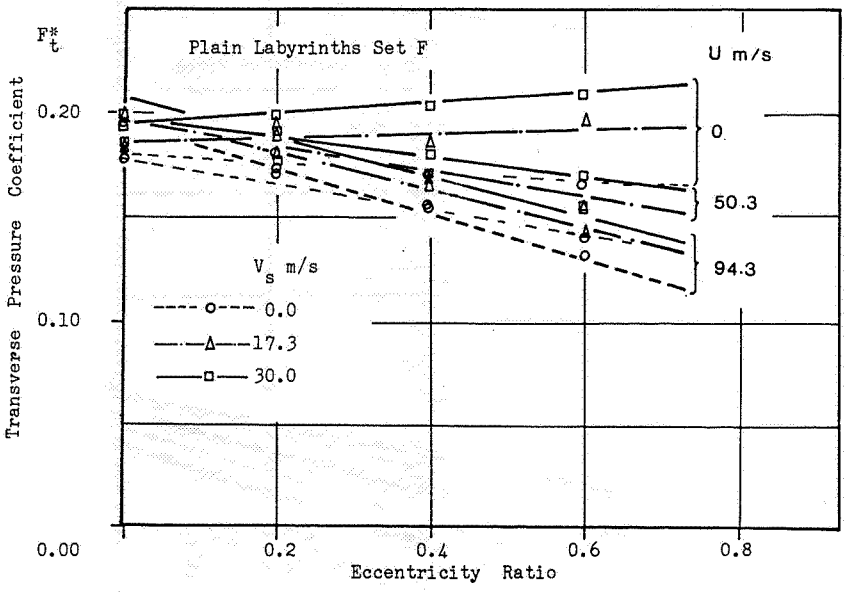

Figure 19. Graphs of dimensionless ratio against eccentricity ratio; set F

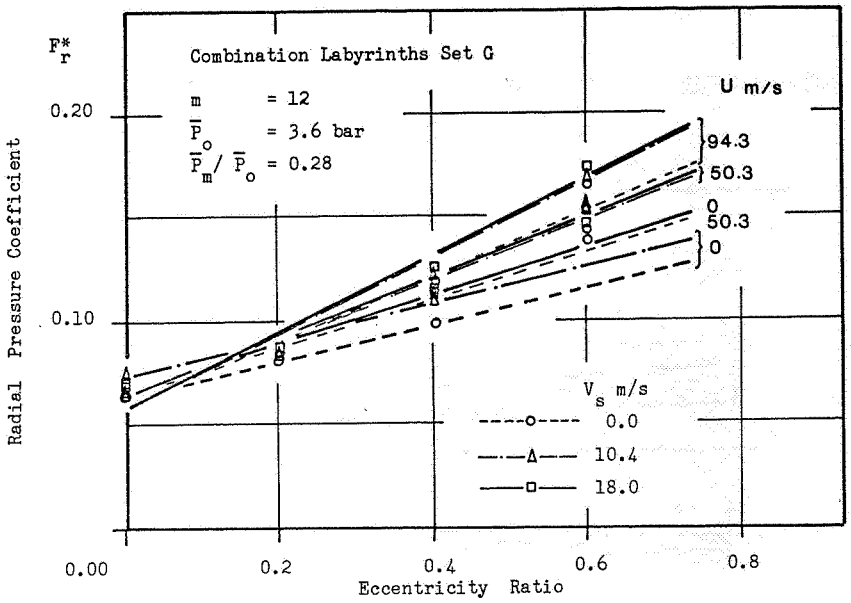

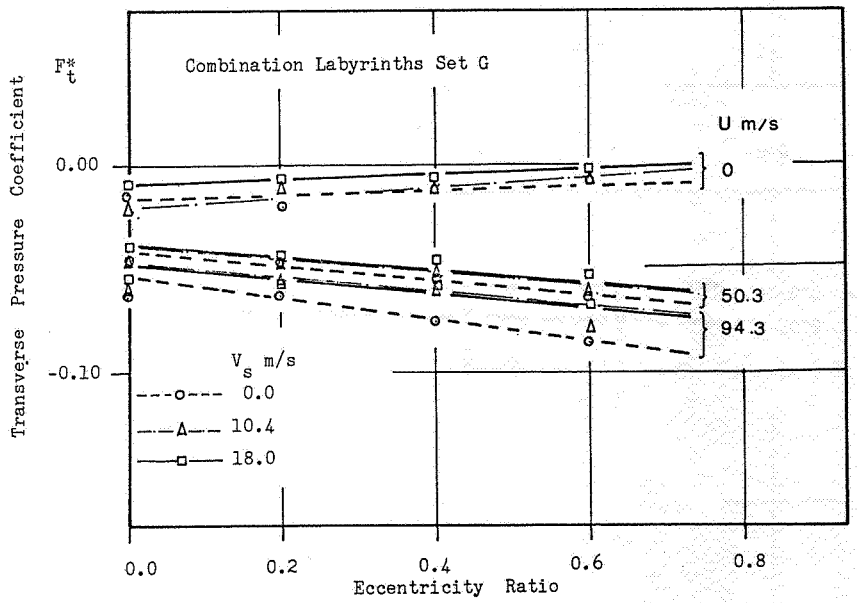

Figure 20. Graphs of dimensionless ratio against eccentricity ratio; set G

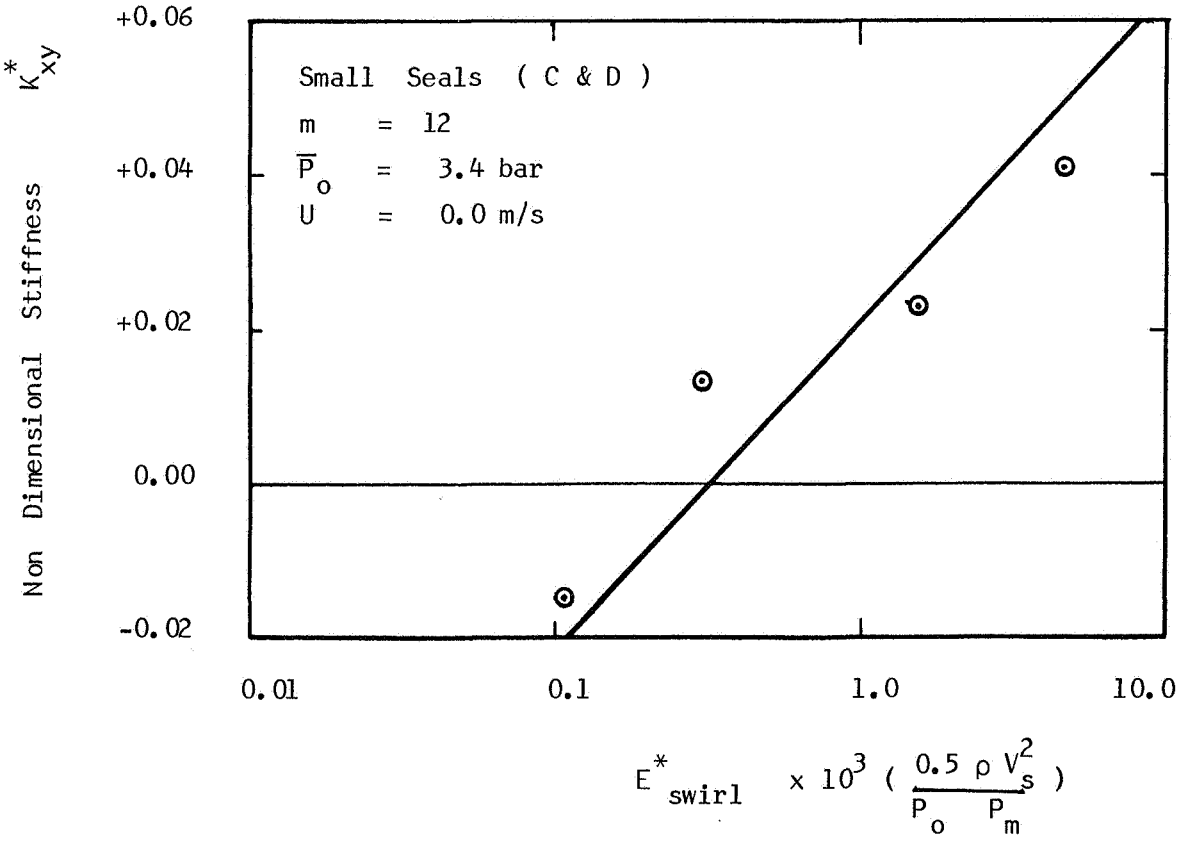

Figure 21. - Variation of cross-coupling with swirl.

ADDITIONAL MATERIAL PRESENT AT WORKSHOP

R.D. Brown J.A. Hart B.E. Falconer

One of the major results from the experimental work was a confirmation that swirl energy was a significant factor in promoting cross-coupling. A rotor kit was adapted as part of an undergraduate project. A plenum chamber was designed around the central mass on a flexible rotor. Four jets in the plenum discharged high velocity air in a tangential direction on the periphery of the central mass. The synchronous critical speed of the rotor was about 3200 r.p.m.

typical results are shown in figures 22 and 23. A gauge pressure of 6 - 8 p.s.i. was maintained in the plenum. Clearly the jet velocity was considerably less than sonic although much greater than the peripheral speed of the rotor.

In both forward and backward flow situations a resonant whip is initiated at a rotor speed between 4500 and 5000 rpm. Thus whirl ratio is between 0.64 and 0.70 considerably greater than 0.5. Typical orbit pattern are shown for 4 revolutions of the rotor. It should be noted that the orbit pattern is not stationary but rotates (as might be expected from the whirl ratio).

These experiments on a small scale rotor provide a laboratory demonstration of high sub-synchronous whirl. The measurements presented here are purely fluid driven, i.e. no physical contact between rotor and stator.

A more sophisticated rig is currently being assembled and experimental results will be reported later.

APPENDIX : Test Seals Data

Set A, B	8.890mm (height) x 9.525 mm (pitch) Fin edge thickness 0.508 mm + 0.050 mm Bore 241.300 mm $\pm$ 0.010 mm Nominal radial clearance 0.635 mm
Set C,D,E,F	4.064 mm x 6.350 mm Fin edge thickness 0.305 mm + 0.050 mm Bore 240.665 mm $\pm$ 0.010 mm Nominal radial clearance 0.381 mm
Set G	4.064 mm, 7.620 mm x 6.350 mm Fin edge thickness 0.305 mm + 0.050 mm Bore (plain seal) 240.665 mm $\pm$ 0.010 mm Bore (split seal) 233.553 mm $\pm$ 0.010 mm Nominal radial clearance 0.381 mm

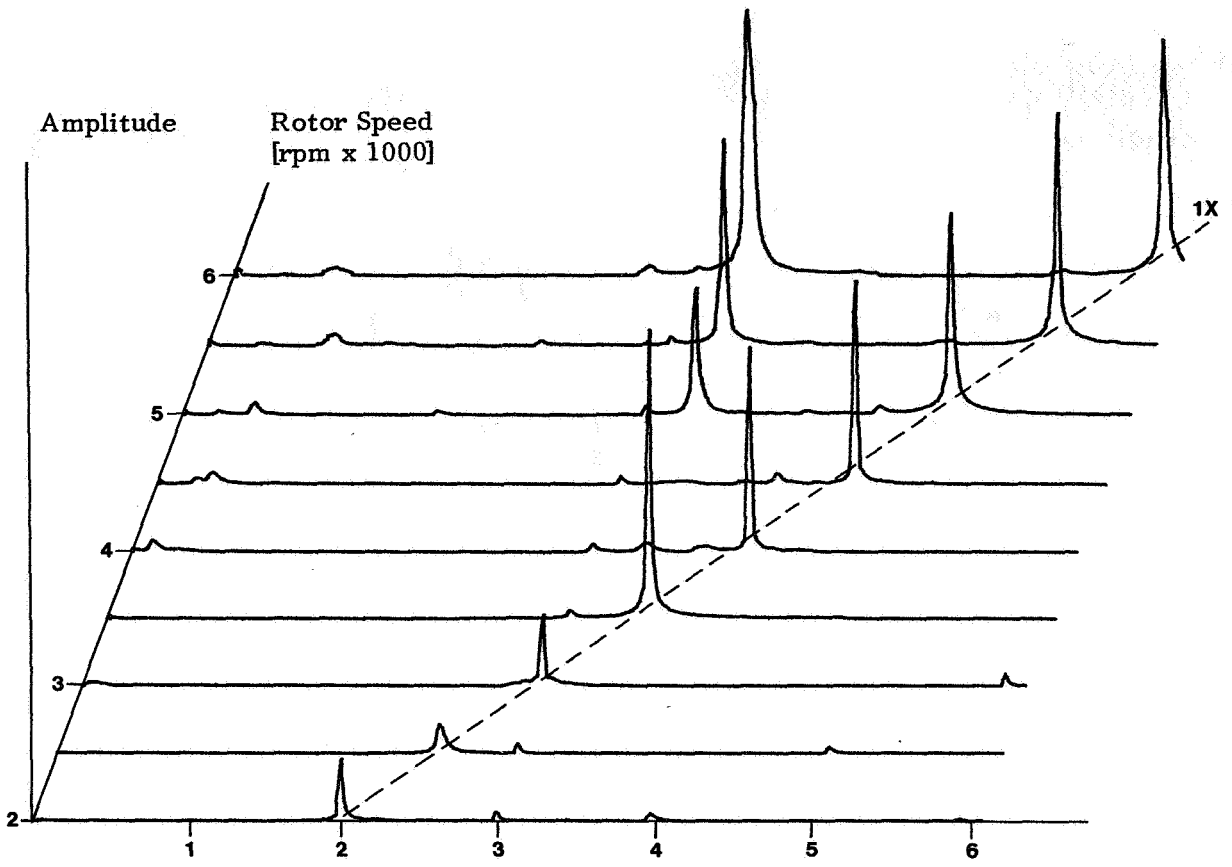

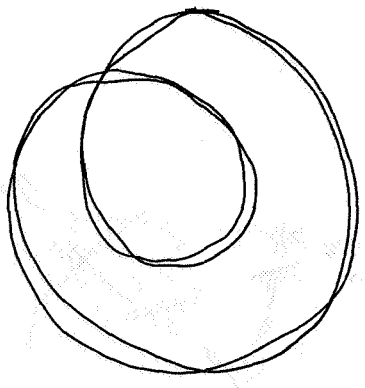

Typical Orbit at 5000 rpm.

Figure 22. - Forward flow.

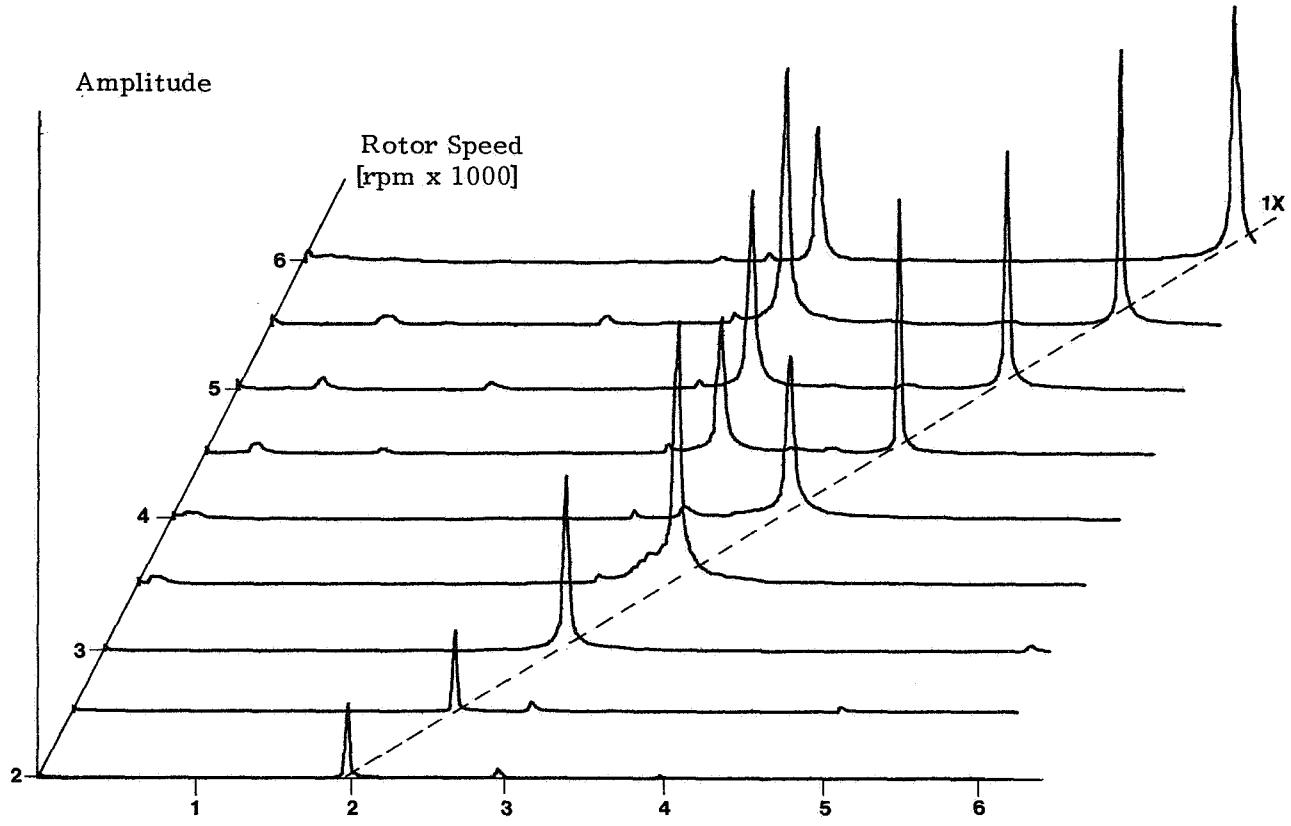

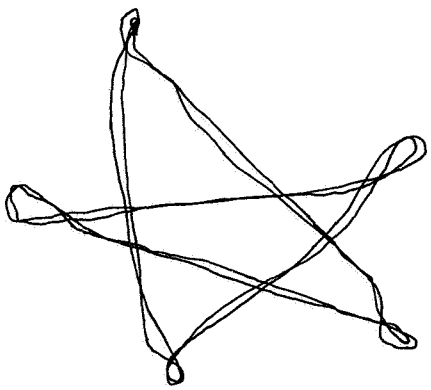

Typical Orbit at 5000 rpm.

Figure 23. - Reverse flow.